

## EARTH SCIENCES

# Diagnosis of CO<sub>2</sub> dynamics and fluxes in global coastal oceans

Zhimian Cao, Wei Yang, Yangyang Zhao, Xianghui Guo, Zhiqiang Yin, Chuanjun Du, Huade Zhao and Minhan Dai\*

## ABSTRACT

Global coastal oceans as a whole represent an important carbon sink but, due to high spatial–temporal variability, a mechanistic conceptualization of the coastal carbon cycle is still under development, hindering the modelling and inclusion of coastal carbon in Earth System Models. Although temperature is considered an important control of sea surface  $p\text{CO}_2$ , we show that the latitudinal distribution of global coastal surface  $p\text{CO}_2$  does not match that of temperature, and its inter-seasonal changes are substantially regulated by non-thermal factors such as water mass mixing and net primary production. These processes operate in both ocean-dominated and river-dominated margins, with carbon and nutrients sourced from the open ocean and land, respectively. These can be conceptualized by a semi-analytical framework that assesses the consumption of dissolved inorganic carbon relative to nutrients, to determine how a coastal system is a CO<sub>2</sub> source or sink. The framework also finds utility in accounting for additional nutrients in organic forms and testing hypotheses such as using Redfield stoichiometry, and is therefore an essential step toward comprehensively understanding and modelling the role of the coastal ocean in the global carbon cycle.

**Keywords:** CO<sub>2</sub> dynamics and fluxes, coastal ocean, ocean-dominated margin, river-dominated ocean margin, carbon cycle

## INTRODUCTION

The coastal ocean, connecting the open ocean and the continents, provides important ecosystem services, particularly as a natural sink of atmospheric CO<sub>2</sub> that contributes to ~20% of the global ocean carbon uptake [1,2]. The coastal ocean is dynamic due to various physical and biogeochemical processes and its fluxes of carbon and other biogenic elements are highly variable in both time and space [3]. Quantifying the inventories and fluxes of coastal ocean carbon, essential for understanding the role of the global carbon cycle in climate variability and change, however, has been a long-standing challenge. As a result, the coastal ocean has been poorly represented in Earth System Models, in terms of both process understanding and temporal–spatial resolution [4,5]. Recent studies have further highlighted the susceptibility of coastal systems to increasingly intensified anthropogenic perturbations [6,7], adding to the challenge of understanding the

already complex coastal carbon cycle and projecting its changes into the future.

Although available research has focused on carbon fluxes across several boundaries at the land–ocean interface, such as estuary–marsh interactions [3,8,9], knowledge of exchanges between ocean margins and the open ocean remains insufficient [3]. Carbon export from the coastal to open ocean was estimated as 0.75 Pg C yr<sup>-1</sup> based on mass balance calculations, but a direct global estimate of the boundary exchanges between the coastal and open ocean is still unattainable due to data paucity [6]. The long-term wintertime data of the partial pressure of CO<sub>2</sub> ( $p\text{CO}_2$ ) suggest a tendency of enhanced uptake of atmospheric CO<sub>2</sub> in many shelf regions [10], which likely exports more dissolved inorganic carbon (DIC) to the open ocean. If this is a global trend, the uptake and export processes in coastal oceans should be included in future models of sea–air CO<sub>2</sub> exchange [7]. In short, more efforts have focused on the river–estuarine input than the fundamental

State Key Laboratory of Marine Environmental Science and College of Ocean and Earth Sciences, Xiamen University, Xiamen 361102, China

\*Corresponding author. E-mail: mdai@xmu.edu.cn

Received 27 March 2019; Revised 21 July 2019; Accepted 23 July 2019

two-way or 3D exchange between ocean margins and the open ocean.

Furthermore, although the CO<sub>2</sub> sink of coastal oceans is approaching a consensus value of 0.15–0.40 Pg C yr<sup>-1</sup>, whether a coastal ocean is a source or a sink of atmospheric CO<sub>2</sub> varies vastly from one coastal system to another [11–19]. Based on a general latitudinal distribution featuring lower seawater *p*CO<sub>2</sub> and thus strong sinks at high latitudes, and high seawater *p*CO<sub>2</sub> and thus sources at low latitudes [12,17,20], temperature-induced changes in the solubility of CO<sub>2</sub> have been considered a major control (i.e. thermal control) of coastal ocean CO<sub>2</sub> fluxes. However, there are also other non-thermal factors at play, particularly water mass mixing (e.g. CO<sub>2</sub> supplied by upwelling) and net primary production, resulting in deviations from this latitudinal distribution [17,19,21]. Understanding these processes in individual systems is a prerequisite for properly modelling the role of the coastal ocean in the global carbon cycle.

Thus, despite great efforts devoted to observing individual coastal systems [22–31] and synthesizing the global coastal CO<sub>2</sub> fluxes [11–19] over the past decades, precisely modelling coastal ocean carbon either using regional models [32] or in a more comprehensive way integrating all domains of Earth's surface [33] remains difficult, mainly due to unknown or oversimplified processes and fluxes in a highly dynamic setting [4,34]. Before an ultimate comprehensive model for predicting future coastal carbon trends at both regional and global scales can be developed, it is useful to establish a conceptual model of the coastal carbon cycle that makes full use of the limited available observations to advance our understanding of physical and biogeochemical processes.

In this study, we show the importance of non-thermal factors on coastal *p*CO<sub>2</sub> and CO<sub>2</sub> fluxes. We establish a semi-analytical framework to understand these non-thermal processes and to diagnose the CO<sub>2</sub> source/sink nature of coastal oceans. By applying the framework to different coastal systems, we highlight the complexity of issues associated with coastal CO<sub>2</sub> dynamics and fluxes, and demonstrate the utility of the framework, particularly in identifying pathways that advance our comprehensive understanding and modelling of the coastal carbon cycle.

## RESULTS AND DISCUSSION

### Non-thermal controls on coastal *p*CO<sub>2</sub>

To illustrate the relative importance of temperature and non-thermal factors to coastal CO<sub>2</sub> dy-

namics and fluxes, we use sea surface temperature (SST), *p*CO<sub>2</sub> and sea–air Δ*p*CO<sub>2</sub> (defined as the difference in *p*CO<sub>2</sub> between the sea and the air, or *p*CO<sub>2,sea</sub> – *p*CO<sub>2,air</sub>) (Fig. 1a–c) data collected at distances of 50 and 100 km from the global shoreline during all four seasons (Supplementary Figs 1, 2 and 3 and Supplementary Section 1.1; see the ‘Methods’ section). Similarly to previous studies synthesizing global coastal CO<sub>2</sub> fluxes [10,17,19], these data mainly represent observations in continental margins consisting of shelf, slope and adjacent marginal seas and excluding nearshore ecosystems in internal waters such as estuaries, lagoons or tidal marshes. While SST clearly shows high values at low latitudes and low values at high latitudes, *p*CO<sub>2</sub> and sea–air Δ*p*CO<sub>2</sub> have a much less defined pattern during each season (Fig. 1a–c and Supplementary Figs 1 and 2). In autumn at 50 km from the shore, for instance, there is no clear latitudinal pattern of *p*CO<sub>2</sub>, with comparable average values between low and high latitudes (Fig. 1b). In the Baltic Sea at ~55°N, *p*CO<sub>2</sub> even approaches 1000 μatm. This leads to extremely high sea–air Δ*p*CO<sub>2</sub> of ~600 μatm, suggesting that this high-latitude coastal system is a CO<sub>2</sub> source (Fig. 1b and c).

In addition to the latitudinal distribution of global coastal *p*CO<sub>2</sub>, which displays a mismatch to that of SST, we quantify the influence of temperature on *p*CO<sub>2</sub> based on the experimental finding that ∂ln*p*CO<sub>2</sub>/∂T is 0.0423°C<sup>-1</sup> for isochemical seawater [35,36]. Because it is nearly impossible to locate an isochemical seawater system, a reasonable approximation is to examine seasonal *p*CO<sub>2</sub> changes in a system with predictable seasonal cycles. Comparing between the observed inter-seasonal *p*CO<sub>2</sub> change (δ*p*CO<sub>2,total,XtoY</sub>; XtoY means from X season to Y season) and the temperature-controlled change (δ*p*CO<sub>2,temp,XtoY</sub>) gives the fractional amount of δ*p*CO<sub>2</sub> that is not controlled by temperature (δ*p*CO<sub>2,others,XtoY</sub>; Equations (1)–(4); see the ‘Methods’ section). We infer that different latitudinal bands vary in their inter-seasonal controls (Fig. 1d and Supplementary Figs 1 and 2).

An examination of the seasonal changes from summer to autumn reveals that non-thermal factors prevail at all latitudinal bands, except from 25° to 35° in both hemispheres (Fig. 1d). This is supported by a statistically significant positive relationship between δ*p*CO<sub>2,total,XtoY</sub> and δ*p*CO<sub>2,others,XtoY</sub> (Fig. 1f). On the other hand, a statistically significant relationship between δ*p*CO<sub>2,total,XtoY</sub> and δ*p*CO<sub>2,temp,XtoY</sub> indicates that decreased SST is associated with enhanced δ*p*CO<sub>2,total,XtoY</sub> (Fig. 1e), contrary to what is expected from the implied thermal control. This is reinforced by aggregating all δ*p*CO<sub>2</sub> data over two consecutive seasons in a full inter-seasonal cycle

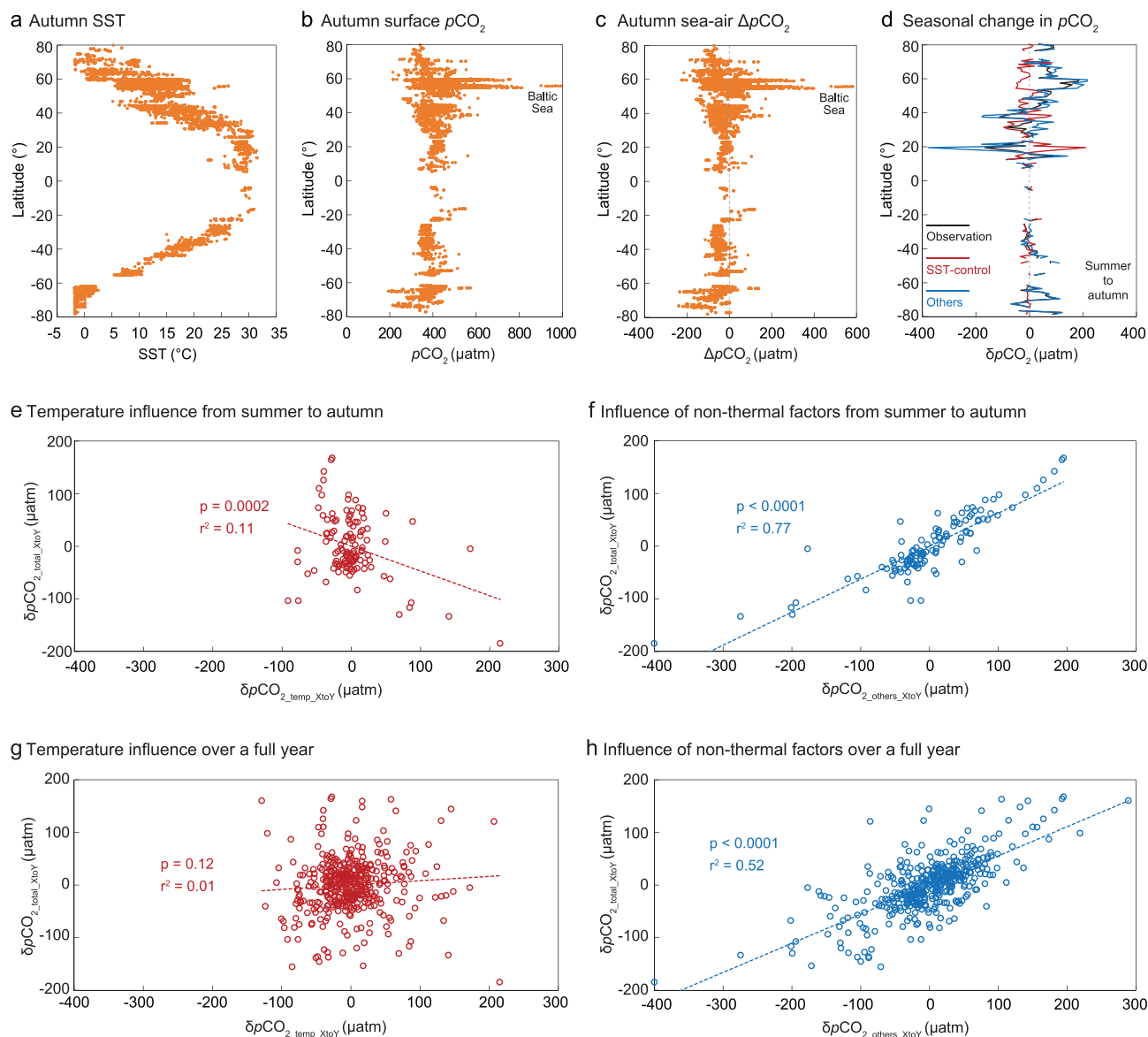


**Figure 1.** Evidence for non-thermal controls on partial pressure of CO<sub>2</sub> (pCO<sub>2</sub>) in global coastal oceans. (a)–(c) Latitudinal distribution of sea surface temperature (SST), surface pCO<sub>2</sub> and sea–air ΔpCO<sub>2</sub> (defined as the difference in pCO<sub>2</sub> between the sea and the air, or pCO<sub>2,sea</sub> – pCO<sub>2,air</sub>) in autumn. (d) Seasonal change in pCO<sub>2</sub> (δpCO<sub>2</sub>) from summer to autumn, averaged over a 1°-latitude band; black, red and blue lines indicate δpCO<sub>2</sub> from field observations (δpCO<sub>2,total,XtoY</sub>; XtoY means from X season to Y season; Equation (1)), solely due to temperature variations (δpCO<sub>2,temp,XtoY</sub>; Equations (2) and (3)) and controlled by other factors (δpCO<sub>2,other,XtoY</sub>; Equation (4)) such as mixing and biogeochemical processes. (e) and (f) Relationship of δpCO<sub>2,total,XtoY</sub> (black curve in (d)) to δpCO<sub>2,temp,XtoY</sub> (red curve in (d)) and δpCO<sub>2,other,XtoY</sub> (blue curve in (d)) from summer to autumn, based on departures from the average, showing that cooler SSTs in fact lead to a higher δpCO<sub>2,total,XtoY</sub>, opposite to the argument of a temperature control over this seasonal transition. Instead, non-thermal factors, such as mixing and biogeochemical processes, control δpCO<sub>2,total,XtoY</sub>. (g) and (h) Relationship of δpCO<sub>2,total,XtoY</sub> to δpCO<sub>2,temp,XtoY</sub> and δpCO<sub>2,other,XtoY</sub> between two consecutive seasons over a full inter-seasonal cycle, based on departures from their respective averages, highlighting an overall lack of control by SST changes but a strong influence of mixing and biogeochemical processes.

(Fig. 1g and h). Compilations of the data at 100 km from the shore give a very similar pattern of pCO<sub>2</sub> in terms of temperature and non-thermal determinations (Supplementary Fig. 2 and Supplementary Section 1.1). Consequently, the inter-seasonal change in global coastal pCO<sub>2</sub> is to a large extent determined by non-thermal factors including water mass mixing and net primary production [17,19,21].

This analysis assumes that coastal systems are isochemical on a global scale; however, such systems are better approximated by more fully characterizing individual ocean margin systems. We thus differentiate the influence of temperature on pCO<sub>2</sub> from the influence of non-thermal factors in the South China Sea and the Arabian Sea (see Supplementary Section 1.2).

In the South China Sea basin, temperature predominantly controls the seasonal  $p\text{CO}_2$  change from winter to spring, but both temperature and non-thermal factors play important roles in the other three inter-seasonal changes. Taking the transition from spring to summer as an example, the temperature increase augments  $p\text{CO}_2$  by  $17 \pm 11 \mu\text{atm}$ , but is offset by the  $p\text{CO}_2$  decrease of  $-23 \pm 17 \mu\text{atm}$  induced by non-thermal factors, leading to a negligible inter-seasonal  $p\text{CO}_2$  change of  $-6 \pm 13 \mu\text{atm}$  (Supplementary Table 1). The latter change mainly reflects physical and biological processes including sea–air exchange, water mass mixing and biological activity.

In the Arabian Sea, the significant seasonal  $p\text{CO}_2$  increase from spring to summer in the coastal area mainly results from the summer upwelling process delivering  $\text{CO}_2$ -rich deep water to the surface; temperature plays a minor role. Moreover, the subsequent decrease in upwelling largely induces the seasonal  $p\text{CO}_2$  decrease from summer to autumn, suggesting that water mass mixing is the major control. In areas without upwelling, both temperature and non-thermal factors play an important role in the inter-seasonal  $p\text{CO}_2$  changes (Supplementary Table 2).

Thus, non-thermal factors—mainly water mass mixing such as upwelling and biological alteration such as net primary production [17,19,21]—play a substantial role in regulating coastal ocean  $p\text{CO}_2$ . The latitudinal distribution of  $p\text{CO}_2$  is obscured by seasonal changes in physical and biogeochemical processes at both river–margin and margin–open ocean interfaces, which cannot be fully simulated even by latest high-resolution models [10,32]; in contrast, such boundary processes are less important for open ocean basins. An alternative way to describe coastal  $\text{CO}_2$  dynamics is therefore required.

### Ocean-dominated margins versus river-dominated ocean margins

To depict the role of water mass mixing and net primary production, we conceptualize the coastal carbon cycle using a semi-analytical framework (see the ‘Methods’ section) that couples physics and biogeochemistry, and DIC and nutrients [16]. Such a semi-analytical framework highlights the boundary processes and aims to resolve the source of DIC and nutrients and their relative consumption via organic carbon production, which determines whether a coastal system is a source (i.e. an excess of DIC during consumption is removed by  $\text{CO}_2$  degassing into the atmosphere) or sink (i.e. a deficit of DIC during consumption is supplied via atmo-

spheric  $\text{CO}_2$  input) of atmospheric  $\text{CO}_2$ . In this context, the world’s coastal oceans are categorized into two distinct regimes: ocean-dominated margin (OceMar) and river-dominated ocean margin (RiOMar) [16,37], with DIC and nutrients sourced from the open ocean and land, respectively. OceMars are characterized by a concurrent non-local input of DIC and nutrients, typically from depth, and the interplay between the externally sourced DIC and nutrients through internal metabolism largely controls the  $\text{CO}_2$  source/sink nature. RiOMars are mostly shelf regions featuring major nutrient loadings from riverine inputs, which include the far-reaching area of river plumes of, for instance, the Amazon [38,39], Yangtze [27,40] and Mississippi [23,41], and exclude nearshore ecosystems such as estuaries, lagoons or tidal marshes. The large river plumes are characterized by high discharges and often show a drawdown of sea surface  $p\text{CO}_2$  resulting from increased net primary production. In these RiOMars, organic carbon production stimulated by riverine nutrients thus outweighs the remineralization of riverine organic matter, leading to sinks of atmospheric  $\text{CO}_2$ .

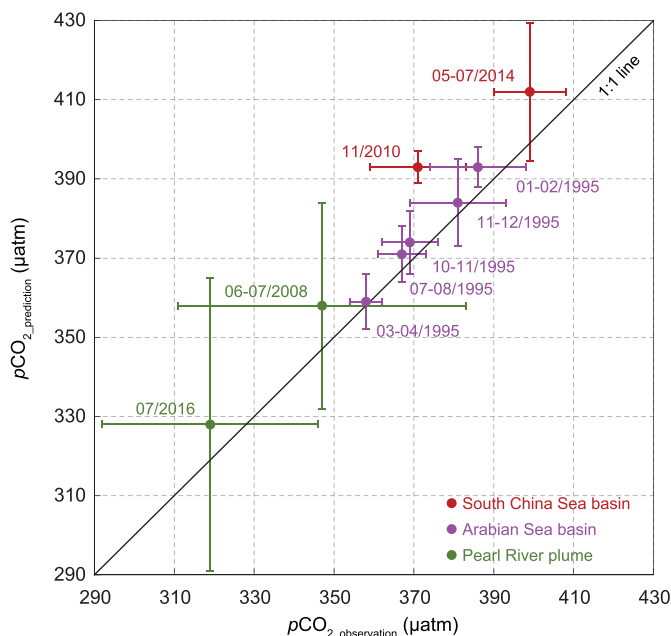
Below, we verify our semi-analytical framework using new datasets compiled from recent observations in the South China Sea, previously identified as a typical OceMar system [16]. We then apply the framework to diagnose the  $\text{CO}_2$  source/sink nature of the Arabian Sea, which is a new OceMar case, and in the Pearl River plume—a major river plume system that is a RiOMar regime.

### OceMar case I: South China Sea basin

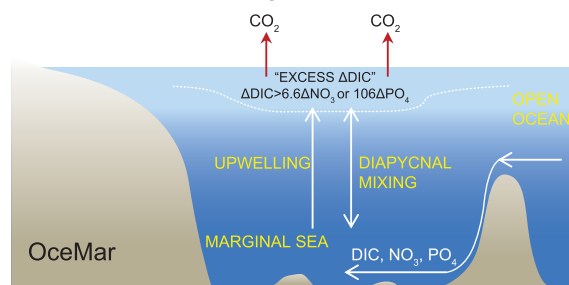
The South China Sea is the largest marginal sea of the North Pacific Ocean and it is an overall source of atmospheric  $\text{CO}_2$  [25]. Our semi-analytical framework has successfully predicted the  $\text{CO}_2$  outgassing in its basin area, consistent with field observations during summer 2009 and spring 2011 [16]. The diapycnal fluxes of materials to the euphotic zone suggest a higher DIC flux relative to phosphate ( $\text{PO}_4$ ) than Redfield stoichiometry [42], further implying DIC excess in the South China Sea [43]. Here, we reassess the  $\text{CO}_2$  source/sink nature using new data collected in autumn (November) 2010 and summer (May–July) 2014 in the South China Sea basin (see Supplementary Section 1.3).

Significant positive relationships between total alkalinity (TAlk) and salinity are observed in the surface mixed layer (<50 m) in both seasons, suggesting a two-endmember mixing scheme between waters immediately below the surface mixed layer and rain water, indicated by near-zero intercepts (Supplementary Fig. 7). Within this scheme, the

## a Verification of framework by observations



## b Processes in OceMar regimes



## c Processes in RiOMar regimes

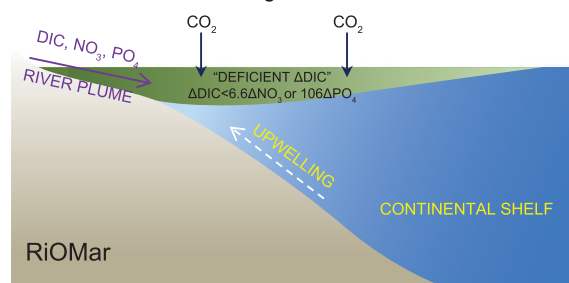


**Figure 2.** Application of our semi-analytical framework to ocean-dominated margins (OceMars) and a river-dominated ocean margin (RiOMar). (a) Verification of predicted  $p\text{CO}_2$  using our semi-analytical framework (see the ‘Methods’ section) versus the observed  $p\text{CO}_2$  in three applications: the South China Sea basin (red, two seasons), Arabian Sea basin (pink, five seasons) and Pearl River plume (green, two seasons). Horizontal and vertical bars represent one standard deviation of  $p\text{CO}_2$  values, reflecting the spatial variability of field observations and variability of our predictions, respectively. The South China Sea basin and the Arabian Sea basin, both diagnosed as a source of atmospheric  $\text{CO}_2$  by our framework, are OceMars. In these systems, DIC and nutrients are mainly from processes at the coastal and open ocean interface, whereby the open ocean-originated DIC,  $\text{NO}_3$  and  $\text{PO}_4$  are transported upward into the surface mixed layer of the marginal sea through vertical mixing and upwelling, as depicted by (b). By contrast, the Pearl River plume, diagnosed as a sink of atmospheric  $\text{CO}_2$  by our framework, is a RiOMar. In these systems, DIC,  $\text{NO}_3$  and  $\text{PO}_4$  mainly originating from rivers are transported along the plume pathway over the continental shelf, whereas contributions from the subsurface water play a minor role, as depicted by (c). The coupled DIC and nutrient consumption via organic carbon production in the surface mixed layer, or in the plume water, ultimately determine the sea–air  $\text{CO}_2$  flux of ocean margins. (b) and (c) are revised from [16].

estimated  $\delta\text{DIC}^*$  based on  $\text{PO}_4$  ( $\delta\text{DIC}^*_{\text{PO}_4}$ ; Equation (11)) is on average  $7 \pm 2 \mu\text{mol kg}^{-1}$  in autumn 2010 and  $17 \pm 9 \mu\text{mol kg}^{-1}$  in summer 2014, which point to excess DIC removed by  $\text{CO}_2$  degassing, and are transformed to a sea–air  $\Delta p\text{CO}_2$  of  $13 \pm 4$  and  $32 \pm 18 \mu\text{atm}$  using Equation (14) (Supplementary Table 3). Combined with the atmospheric  $p\text{CO}_2$  field observations of  $\sim 380 \mu\text{atm}$  in both seasons, the sea surface  $p\text{CO}_2$  (Equation (15)) in the South China Sea basin is predicted to be  $393 \pm 4 \mu\text{atm}$  in autumn 2010 and  $412 \pm 18 \mu\text{atm}$  in summer 2014, consistent with, if only slightly higher than, the field observations of  $371 \pm 12$  and  $399 \pm 9 \mu\text{atm}$  (red-filled circles, Fig. 2a; Supplementary Fig. 8). Note that the estimated sea surface  $p\text{CO}_2$  based on nitrate ( $\text{NO}_3$ ) is essentially consistent with that based on  $\text{PO}_4$  in both seasons, which is discussed later. We thus confirm the  $\text{CO}_2$  source nature of the South China Sea.

The main processes involved in an OceMar regime are depicted in Fig. 2b. DIC and nutrients are mainly sourced from the open ocean. Through

vertical mixing and upwelling, such open ocean-originated DIC,  $\text{NO}_3$  and  $\text{PO}_4$  are transported upward into the surface mixed layer, in which the consumption of DIC relative to nutrients determines whether DIC is in excess or in deficit relative to the external input. The excess DIC, as diagnosed in the South China Sea basin, is eventually released to the atmosphere, making the region a  $\text{CO}_2$  source.

### OceMar case II: Arabian Sea basin

The Arabian Sea is characterized by strong seasonal cycles driven by the Asian Monsoon. There is well-defined upwelling during the southwest monsoon season due to offshore Ekman transport, which often manifests as low SST along the Arabian Peninsula [44]. The upwelling results in increased biological productivity and complicated  $p\text{CO}_2$  responses. Using the carbonate system and nutrient data collected in 1995 from five cruises in winter (January–February and November–December) during the northeast monsoon season, in spring (March–April)

and autumn (October–November) during the inter-monsoon season and in summer (July–August) during the southwest monsoon season (see Supplementary Section 1.4), we estimate the CO<sub>2</sub> source/sink nature in the Arabian Sea.

Talk and salinity in the surface mixed layer (<75–100 m) show significant positive relationships in all seasons, suggesting an overall two-endmember mixing scheme between waters immediately below the surface mixed layer and rain water (indicated by near-zero intercepts) or a non-zero-solute freshwater (indicated by substantive intercepts) (Supplementary Fig. 10). Within this scheme, the average  $\delta\text{DIC}^*_{\text{PO}_4}$  values are estimated to be  $23 \pm 3$  (January–February),  $4 \pm 5$  (March–April),  $20 \pm 5$  (July–August),  $25 \pm 6$  (October–November) and  $26 \pm 8$  (November–December)  $\mu\text{mol kg}^{-1}$ , which point to excess DIC removed by CO<sub>2</sub> degassing and are transformed to a sea–air  $\Delta p\text{CO}_2$  of  $37 \pm 5$ ,  $6 \pm 7$ ,  $30 \pm 7$ ,  $37 \pm 8$  and  $39 \pm 11$   $\mu\text{atm}$  using Equation (14) (Supplementary Table 3). Sea surface  $p\text{CO}_2$  (Equation (15)) estimated for the five consecutive seasons are  $393 \pm 5$ ,  $359 \pm 7$ ,  $371 \pm 7$ ,  $374 \pm 8$  and  $384 \pm 11$   $\mu\text{atm}$ . The field-observed  $p\text{CO}_2$  values are  $386 \pm 12$ ,  $358 \pm 4$ ,  $367 \pm 6$ ,  $369 \pm 7$  and  $381 \pm 12$   $\mu\text{atm}$ , which agree rather well with the predicted results (pink-filled circles, Fig. 2a; Supplementary Fig. 11). Note that our analysis based on NO<sub>3</sub> is, within error, comparable to that based on PO<sub>4</sub> during the five seasons, which is discussed later. While the sea surface  $p\text{CO}_2$  equals the air  $p\text{CO}_2$  in the spring inter-monsoon season, in other seasons, the Arabian Sea must have acted as a weak source of CO<sub>2</sub> to the atmosphere (Fig. 2b).

### RiOMar case: Pearl River plume

The Pearl River is one of the world's major rivers, discharging  $3.26 \times 10^{11}$  m<sup>3</sup> of freshwater annually and forming a river plume over the broad continental shelf of the northern South China Sea in summer. This river plume, travelling along with the coastal current, extends to hundreds of kilometres from the mouth of the Pearl River estuary and strongly modulates the shelf biogeochemistry [45–47]. Here, we use datasets collected on the northern South China Sea shelf in the summers of 2008 (June–July) and 2016 (July) to evaluate the CO<sub>2</sub> source/sink nature of the Pearl River plume waters with salinities <33.0 (see Supplementary Section 1.5).

Due to the co-influence of both the river plume and coastal upwelling in both seasons, a three-endmember mixing scheme in the upper 100 m is identified between the plume water, offshore subsurface water and offshore surface water, as suggested by the temperature–salinity relationship (Supple-

mentary Fig. 13). Within this scheme, the estimated  $\delta\text{DIC}^*$ , based on NO<sub>3</sub> ( $\delta\text{DIC}^*_{\text{NO}_3}$ ; Equation (10)), is on average  $-6 \pm 13$   $\mu\text{mol kg}^{-1}$  in summer 2008 and  $-34 \pm 20$   $\mu\text{mol kg}^{-1}$  in summer 2016, which indicates a DIC deficit supplied via atmospheric CO<sub>2</sub> inputs, and these values are transformed to a sea–air  $\Delta p\text{CO}_2$  of  $-12 \pm 26$  and  $-62 \pm 37$   $\mu\text{atm}$  using Equation (13) (Supplementary Table 3). Combined with the field-observed atmospheric  $p\text{CO}_2$  of  $\sim 370$  and  $\sim 390$   $\mu\text{atm}$  during the two seasons, the sea surface  $p\text{CO}_2$  was estimated to be  $358 \pm 26$  and  $328 \pm 37$   $\mu\text{atm}$  (Equation (15)); both values are consistent with the calculated  $p\text{CO}_2$  of  $347 \pm 36$  and  $319 \pm 27$   $\mu\text{atm}$  using DIC and Talk data (green-filled circle, Fig. 2a; Supplementary Fig. 14). We thus demonstrate that the Pearl River plume is a sink of atmospheric CO<sub>2</sub>, which was stronger in summer 2016 than in summer 2008. However, our analysis based on PO<sub>4</sub> suggests it was a CO<sub>2</sub> source during both seasons. This inconsistency is examined later.

The main processes involved in a RiOMar regime are depicted in Fig. 2c. DIC and nutrients are mainly sourced from the river and transported along the plume pathway on the continental shelf. As in OceMars, the consumption of DIC relative to nutrients in the plume water determines whether DIC is in excess or in deficit. A DIC deficit, as identified in the Pearl River plume, is supplied by atmospheric CO<sub>2</sub> inputs, making the region a CO<sub>2</sub> sink.

Thus, we successfully extend the applicability of the semi-analytical framework from OceMars to RiOMars, helping to better characterize the coastal carbon cycle and resolve the CO<sub>2</sub> dynamics and fluxes in a quantitative way. While the major source of DIC and nutrients differs between the two coastal systems due to different boundary processes, the same metabolic process coupling the externally supplied DIC and nutrients modulates the sea–air CO<sub>2</sub> exchange in both regimes (Fig. 2b and c).

### Utilities and uncertainties

Our framework (see the 'Methods' section) characterizes two important carbon processes that are independent of temperature, namely physical and biogeochemical processes, in the coupled DIC–nutrient dynamics. Application of the framework strengthens the notion that, even though global coastal oceans are a sink of atmospheric CO<sub>2</sub> as a whole, individual coastal systems are highly variable, may act as CO<sub>2</sub> sources or sinks and need to be characterized individually. In addition to the three cases we presented here, other successful applications of our framework include the Caribbean Sea

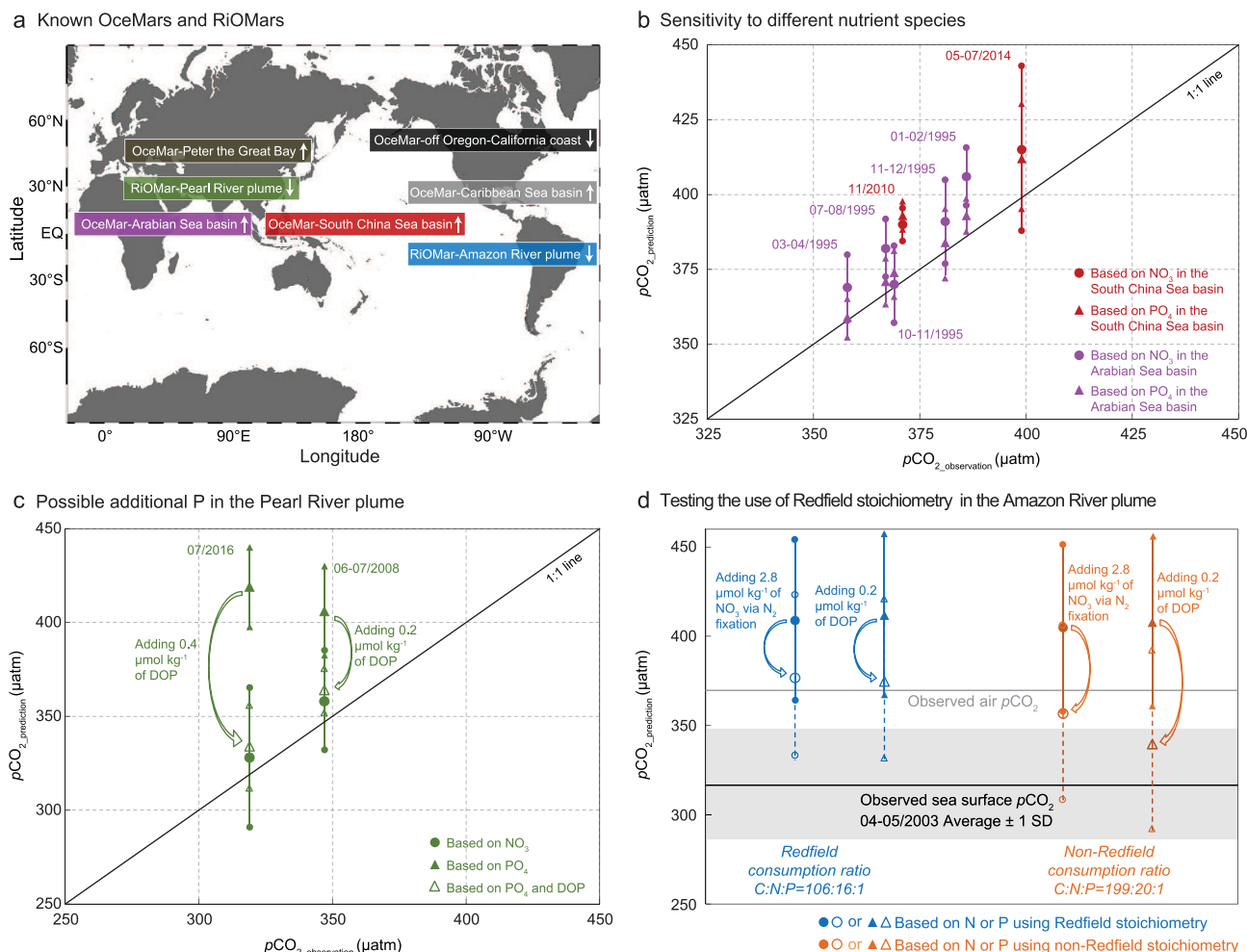


**Figure 3.** Utilities and uncertainties of our semi-analytical diagnostic framework in OcéMar and RiOMar regimes. (a) Known OcéMars and RiOMars, with upward and downward arrows indicating sources and sinks of atmospheric CO<sub>2</sub>, respectively. (b) Comparison between predicted  $p\text{CO}_2$  based on different nutrient species and observed  $p\text{CO}_2$  in the South China Sea basin (red, two seasons) and the Arabian Sea basin (pink, five seasons). The diagonal line indicates a perfect fit between the diagnosed and observed values, and vertical bars represent one standard deviation (1 SD) of the diagnosed  $p\text{CO}_2$  values, which are largely due to the spatial variability of the observations. The consistency between CO<sub>2</sub> source or sink diagnoses based on NO<sub>3</sub> or PO<sub>4</sub> demonstrates insensitivity to the choice of nutrient species. (c) As in (b), but for the Pearl River plume (green, two seasons); in both seasons, our framework identifies an addition of P that is not accounted for by our observations but needs to be considered to bring the predicted  $p\text{CO}_2$  to that based on NO<sub>3</sub>. The added P is likely transformed from dissolved organic phosphorus (DOP). (d) As in (b), but for the Amazon River plume (blue, one season), which our framework diagnoses as a source, opposite to the observed sink. Under the Redfield stoichiometry, even with unaccounted-for N or P added, our framework still predicts a sea surface  $p\text{CO}_2$  (blue) higher than the observed air  $p\text{CO}_2$  (grey line) but, under a non-Redfield stoichiometry, the same added nutrients lead to a predicted  $p\text{CO}_2$  (orange) that is close to or within the uncertainty range due to spatial variability (grey shadow) of the observed average sea surface  $p\text{CO}_2$  (black line).

basin [16], the upwelling system of the US west coast off Oregon and California [48] and the Peter the Great Bay of the Japan/East Sea [30] (Fig. 3a). These are identified as OcéMars and can be either a CO<sub>2</sub> source or sink. However, for the Amazon River plume, a typical RiOMar system (Fig. 3a), our prediction as a source differs from observations as a sink. This is examined later.

The semi-analytical framework follows Redfield stoichiometry, in which the C, N and P consumption ratio is constant at 106:16:1 [42]. Treating this ratio as a global or regional constant is mostly acceptable

in the context of interpreting snapshots of the water column [49]. However, higher DIC/NO<sub>3</sub> consumption ratios than Redfield stoichiometry have been observed, probably resulting from DIC over-consumption relative to inorganic N via the production of dissolved organic matter (DOM) [50]. This suggests that the assumption of a Redfield consumption ratio may not be always valid and must be verified. On the other hand, some of the unaccounted-for nutrients may also result in an apparently higher DIC/NO<sub>3</sub>, DIC/PO<sub>4</sub> or NO<sub>3</sub>/PO<sub>4</sub> consumption ratio [46].

Application of our framework to the South China Sea and the Arabian Sea illustrates that, when all nutrients are accounted for, our analysis is robust and insensitive to the choice of nutrient species. In the South China Sea basin, the estimated  $\delta\text{DIC}^*_{\text{NO}_3}$  agrees well with the  $\delta\text{DIC}^*_{\text{PO}_4}$  in both autumn 2010 and summer 2014, resulting from an average  $\Delta\text{NO}_3/\Delta\text{PO}_4$  ratio (i.e. the apparent biological consumption of  $\text{NO}_3$  relative to  $\text{PO}_4$  obtained by Equation (8)/Equation (9)) close to the Redfield value of 16 (Supplementary Table 3). Accordingly, the estimated  $p\text{CO}_2$  values based on  $\delta\text{DIC}^*_{\text{NO}_3}$  and  $\delta\text{DIC}^*_{\text{PO}_4}$ , respectively, are within error, comparable to each other during both seasons (red-filled symbols, Fig. 3b). In the Arabian Sea basin, the estimated  $p\text{CO}_2$  based on  $\delta\text{DIC}^*_{\text{NO}_3}$  is also within the uncertainty range of that based on  $\delta\text{DIC}^*_{\text{PO}_4}$ , and both are consistent with field observations during the five seasons analysed (pink-filled symbols, Fig. 3b), when the  $\Delta\text{NO}_3/\Delta\text{PO}_4$  ratios are equal to the Redfield value (Supplementary Table 3). The consistency between results from the two nutrient species suggests that consumption of C/N and C/P are well coupled in these two OcéMar systems, which points to the robustness of our framework and strengthens the validity of using Redfield stoichiometry in these cases.

In the Pearl River plume, however, the estimated  $\delta\text{DIC}^*_{\text{PO}_4}$  values are positive in both the summers of 2008 and 2016 based on our own observations, which would imply a  $\text{CO}_2$  source (large green-filled triangles, Fig. 3c), opposite to the direction of the  $\text{CO}_2$  flux based on  $\delta\text{DIC}^*_{\text{NO}_3}$  (large green-filled circles, Fig. 3c). This discrepancy is supported by much higher  $\Delta\text{NO}_3/\Delta\text{PO}_4$  ratios than the Redfield value (Supplementary Table 3), suggesting that an additional source of P not accounted for by our observations is needed to balance the  $\text{NO}_3$ -based  $\delta\text{DIC}^*$  and thus reduce the estimated  $p\text{CO}_2$  toward that based on  $\delta\text{DIC}^*_{\text{NO}_3}$  or field observations. This amount of P is estimated to be  $\sim 0.2$  and  $\sim 0.4 \mu\text{mol kg}^{-1}$  for the summers of 2008 and 2016, respectively. Once added, the calculated  $p\text{CO}_2$  (large green-unfilled triangles, Fig. 3c) is close to the observed  $p\text{CO}_2$ . The additional P can be transformed from dissolved organic phosphorus (DOP) during metabolic processes [46]. This finding of unaccounted-for DOP is confirmed by an independently observed value of approximately  $0.5 \mu\text{mol kg}^{-1}$  in the upstream Pearl River estuary in summer 2015 [51], highlighting a utility of our framework.

Nevertheless, there is at least one case—the Amazon River plume—in which, even after accounting for additional nutrients, the predicted and observed results of sea surface  $p\text{CO}_2$  still differ. In this case, the debate regarding the validity of Redfield stoichiometry continues [50,52]. Here, using avail-

able observations of DIC,  $\text{NO}_3$  and  $\text{PO}_4$  (see Supplementary Section 1.6), our framework determines that the Amazon River plume (salinities  $\sim 30.0$ – $35.0$ ) is a source of atmospheric  $\text{CO}_2$ , whereas observations from April–May 2003 show it acts as a sink [38,39].

To be consistent, it would require a  $\text{NO}_3$  consumption of  $\sim 7.4 \mu\text{mol kg}^{-1}$  to meet the DIC removal and drawdown of  $p\text{CO}_2$ . The estimated  $\Delta\text{NO}_3$  using our framework (Equation (8)) is, however, only  $\sim 1.0 \mu\text{mol kg}^{-1}$  (the resulting prediction of  $p\text{CO}_2$  is denoted by a large blue-filled circle, Fig. 3d), suggesting that the majority of  $\text{NO}_3$  ( $\sim 6.4 \mu\text{mol kg}^{-1}$ ) needs to be supplied from additional sources, such as  $\text{N}_2$  fixation. Strong  $\text{N}_2$  fixation was consistently observed in the Amazon River plume [53–55], estimated to be  $1404.6 \mu\text{mol N m}^{-2} \text{d}^{-1}$  in the mesohaline zone with salinities of 30.0–35.0 [56]. Combined with a mixed layer depth of  $\sim 20$  m and a water residence time of  $\sim 40$  days, the total N supplied by  $\text{N}_2$  fixation would only be  $2.8 \mu\text{mol kg}^{-1}$ , of which just a fraction could be directly transformed to  $\text{NO}_3$  and subsequently consumed during primary production. Even taking this value as a maximum of  $\text{NO}_3$  added, the resulting prediction of sea surface  $p\text{CO}_2$  is still higher than the field-observed atmospheric  $p\text{CO}_2$  (the former denoted by a large blue-unfilled circle, Fig. 3d). We therefore use another nutrient species, i.e.  $\text{PO}_4$ , which leads to a finding that the estimated  $\Delta\text{PO}_4$  (Equation (9)) is only  $\sim 0.02 \mu\text{mol kg}^{-1}$  (the resulting prediction of  $p\text{CO}_2$  is denoted by a large blue-filled triangle, Fig. 3d) and additional  $\text{PO}_4$  of  $0.53 \mu\text{mol kg}^{-1}$  is needed to predict the  $\text{CO}_2$  sink. DOP, with a concentration of up to  $0.2 \mu\text{mol kg}^{-1}$ , is the dominant species of P [57] (the resulting prediction of  $p\text{CO}_2$  is denoted by a large blue-unfilled triangle, Fig. 3d), which is still not sufficient to support the DIC consumption.

Although  $\text{N}_2$  fixation and DOP utilization may partially be responsible for the low  $\text{NO}_3$  and  $\text{PO}_4$  removal relative to DIC, including them in the semi-analytical framework seems incapable of reversing the prediction of their  $\text{CO}_2$  source/sink nature. We envisage that this could be a case in which Redfield stoichiometry is not fully valid. If DIC overconsumption occurred via the DOM production with higher C:N:P stoichiometry (199:20:1) [58], this would also lead to the overestimated  $\delta\text{DIC}^*_{\text{NO}_3}$  and  $\delta\text{DIC}^*_{\text{PO}_4}$  (Equations (10) and (11)). By considering both unaccounted-for nutrients and the non-Redfield stoichiometry of DOM, we can resolve the sea–air  $\Delta p\text{CO}_2$  close to the  $\text{CO}_2$  sink nature of the Amazon River plume. In particular, the estimated  $p\text{CO}_2$  based on P is closer to the field-observed range of  $p\text{CO}_2$  (orange symbols, Fig. 3d). Nevertheless, this is obviously an oversimplification because DIC



and inorganic nutrients are not merely transformed into DOM during biological consumption. The realistic C, N and P consumption ratio would lie in between, pointing to an uncertainty of our estimation, which warrants further study.

## SUMMARY

Although global coastal oceans as a whole have been recognized as an important natural sink of atmospheric CO<sub>2</sub>, the associated physical and biogeochemical processes need to be better understood. Our finding that inter-seasonal changes of global coastal pCO<sub>2</sub> are strongly determined by non-thermal factors has led to the establishment of our semi-analytical framework, which conceptualizes the role of water mass mixing and net primary production. The framework diagnoses CO<sub>2</sub> dynamics and fluxes in coastal oceans in two distinctive regimes, i.e. OceMars and RiOMars. We show that coastal oceans as a CO<sub>2</sub> sink mostly refers to RiOMars, but OceMars can be either a source or sink: e.g. the South China Sea basin is a source whereas the Oregon–California coast is a sink. Therefore, the details are critical and must be captured correctly by any global carbon cycle models, which has been a long-standing scientific challenge.

It is in this context that our framework has found utility while contributing to the scientific debate. On the one hand, when validated by independent observations, it helps account for additional nutrients as is the case in the Pearl River plume. On the other hand, it helps test the validity of Redfield stoichiometry as is the case in the Amazon River plume. We anticipate that the usefulness of our developed framework will inspire future studies. One natural next step would be to apply this framework to other global coastal systems. To this end, observations of DIC and nutrients from likely sources are essential, but this is not a trivial effort. International collaboration is crucial in order to gain the global picture that is composed of detailed characteristics of individual coastal ocean systems. This would also increase understanding of the associated processes, and their parameterization for inclusion in models: either mechanistic, such as our framework, or as a comprehensive global system [33], the latter being the ultimate goal of future research efforts.

## METHODS

### Global coastal pCO<sub>2</sub> data sources and analysis

Global coastal SST and pCO<sub>2</sub> data employed in Fig. 1 and Supplementary Figs 1 and 2 were

extracted from the Surface Ocean CO<sub>2</sub> Atlas (<http://www.socat.info/>). We selected pCO<sub>2</sub> values at the distance of 50 and 100 km from major land masses in the SOCAT v3.0 data product [59], which cover latitudes from 82°N to 78°S and years from 1962 to 2014 (Supplementary Fig. 3).

Data analysis was based on 1°-latitude averages. To differentiate the influence of temperature on seasonal pCO<sub>2</sub> variations from all other influences, we first calculated the total variation of field-observed pCO<sub>2</sub> from X season to Y season ( $\delta pCO_{2\_total\_XtoY}$ ) according to Equation (1):

$$\delta pCO_{2\_total\_XtoY} = pCO_{2\_Y} - pCO_{2\_X}. \quad (1)$$

pCO<sub>2\_X</sub> and pCO<sub>2\_Y</sub> are the 1°-latitude averaged field-observed pCO<sub>2</sub> in X season and Y season, respectively. We then defined  $\delta pCO_{2\_temp\_XtoY}$  as the pCO<sub>2</sub> variation solely induced by temperature changes from X season to Y season, which was calculated as:

$$\delta pCO_{2\_temp\_XtoY} = pCO_{2\_@Ytemp} - pCO_{2\_X}. \quad (2)$$

pCO<sub>2\_@Ytemp</sub> is the theoretical pCO<sub>2</sub> value during Y season considering only temperature changes relative to X season, which was calculated according to Equation (3) [36]:

$$pCO_{2\_@Ytemp} = pCO_{2\_X} \times \exp [0.0423 \times (temp\_Y - temp\_X)]. \quad (3)$$

temp<sub>X</sub> and temp<sub>Y</sub> are the 1°-latitude averaged SSTs during seasons X and Y, respectively. Finally, the difference between  $\delta pCO_{2\_total\_XtoY}$  and  $\delta pCO_{2\_temp\_XtoY}$  ( $\delta pCO_{2\_others\_XtoY}$ ; Equation (4)) reflects the pCO<sub>2</sub> variability between seasons X and Y resulting from other processes (e.g. water mass mixing and net primary production) beyond the temperature effect.

$$\delta pCO_{2\_others\_XtoY} = \delta pCO_{2\_total\_XtoY} - \delta pCO_{2\_temp\_XtoY}. \quad (4)$$

The four seasonal transitions presented in Supplementary Figs 1 and 2 are changes sequentially from winter (X) to spring (Y), from spring (X) to summer (Y), from summer (X) to autumn (Y) and from autumn (X) to winter (Y). Seasons are defined as March, April and May as spring in the Northern Hemisphere and September, October and November as spring in the Southern Hemisphere.

## Semi-analytical diagnostic framework of CO<sub>2</sub> dynamics and fluxes in ocean margins

Our diagnostic framework uses the mass balance of DIC in the surface mixed layer (Equation (5)):

$$\frac{\partial DIC}{\partial t} = \sum F_{DIC} - NEC - NEP - F_{CO_2}. \quad (5)$$

Here, *NEC* is the net ecosystem calcification and *NEP* is the net ecosystem production.  $F_{DIC}$  is the external DIC input to the surface mixed layer and  $F_{CO_2}$  is the sea–air CO<sub>2</sub> flux. At steady state and assuming negligible net calcification often suggested by conservative TALK distributions, Equation (5) can be simplified to Equation (6):

$$F_{CO_2} = \sum F_{DIC} - NEP. \quad (6)$$

The sea–air CO<sub>2</sub> flux is thus a function of the sum of DIC inputs and net ecosystem production, or the CO<sub>2</sub> is a net consequence of externally transported DIC and internal metabolic CO<sub>2</sub> consumption. However, resolving Equation (6) is not a trivial task, as it requires a full solution to the 3D ocean circulation that is not always possible. Here, we couple the physical transport and biological mediation of DIC and nutrients (i.e. NO<sub>3</sub> and PO<sub>4</sub>) within comparable timescales, by establishing a water mass mixing scheme in order to define the physical transport, or the conservative portion of DIC and nutrients from the adjacent water masses, and the constraint of the biogeochemical alteration of these non-local inputs in the upper water column of ocean margins [16]. These processes are described by

$$\Delta DIC = DIC_{cons} - DIC_{meas}, \quad (7)$$

$$\Delta NO_3 = NO_{3\_cons} - NO_{3\_meas}, \quad (8)$$

$$\Delta PO_4 = PO_{4\_cons} - PO_{4\_meas}. \quad (9)$$

The subscripts ‘cons’ and ‘meas’ in Equations (7)–(9) denote conservative-mixing-induced and field-observed values, respectively. The difference between them, represented as  $\Delta$ , is the addition (negative values resulting from organic matter remineralization outweighing primary production) or removal (positive values resulting from primary production outweighing organic matter remineralization) of DIC, NO<sub>3</sub> or PO<sub>4</sub> beyond the mixing control. In the latter case, we subsequently use  $\delta DIC^*$  to quantify the consumption of DIC relative to nutrients based on the classic Redfield stoichiometry of C:N:P = 106:16:1 (Equations (10) and

(11)) [42], which determines whether DIC is in excess (i.e.  $\delta DIC^* > 0$ ) or in deficit (i.e.  $\delta DIC^* < 0$ ) relative to nutrients in the seawater body:

$$\delta DIC^* = \Delta DIC - 6.6 \Delta NO_3, \quad (10)$$

$$\delta DIC^* = \Delta DIC - 106 \Delta PO_4. \quad (11)$$

Under steady-state conditions over a relatively long timescale (e.g. seasonal scale), such excesses or deficits in DIC would be degassed (i.e. CO<sub>2</sub> source) or compensated (i.e. CO<sub>2</sub> sink) by sea–air CO<sub>2</sub> gas exchange. At the same time, only a fraction of  $\delta DIC^*$  is involved in the gas exchange, depending on the Revelle factor (RF), which is referred to as the fractional change in surface seawater CO<sub>2</sub> ( $\partial pCO_2/pCO_2$ ) over the fractional change in DIC ( $\partial DIC/DIC$ ) at a given temperature, salinity and TALK (Equation (12)) [60,61]. In other words, RF quantifies the ocean’s sensitivity to an increase in atmospheric CO<sub>2</sub>, i.e.

$$RF = \frac{\partial pCO_2/pCO_2}{\partial DIC/DIC}. \quad (12)$$

In a simplified way and as an approximation,  $\partial DIC$  equals  $\delta DIC^*$ , which is solely achieved through sea–air CO<sub>2</sub> exchange, implying that  $\partial pCO_2$  may represent the sea–air  $\Delta pCO_2$  (defined as the difference in  $pCO_2$  between the sea and the air, or  $pCO_{2\_sea} - pCO_{2\_air}$ ). Given an initial balance of CO<sub>2</sub> between the seawater and the atmosphere, the sea–air  $\Delta pCO_2$  is obtained by

$$\begin{aligned} \Delta pCO_2 &= RF \times pCO_{2\_air} \times \frac{\delta DIC^*}{DIC} \\ &= RF \times pCO_{2\_air} \times \frac{\Delta DIC - 6.6 \Delta NO_3}{DIC}, \end{aligned} \quad (13)$$

$$\begin{aligned} \Delta pCO_2 &= RF \times pCO_{2\_air} \times \frac{\delta DIC^*}{DIC} \\ &= RF \times pCO_{2\_air} \times \frac{\Delta DIC - 106 \Delta PO_4}{DIC}. \end{aligned} \quad (14)$$

The surface  $pCO_2$  in the seawater body can thus be predicted as

$$pCO_{2\_sea\_pred} = pCO_{2\_air} + \Delta pCO_2. \quad (15)$$

## SUPPLEMENTARY DATA

Supplementary data are available at [NSR](#) online.

## ACKNOWLEDGEMENTS

We thank L. Wang, T. Huang, L. Guo, Y. Xu, Y. Li, J. Hu and D. Wang for assistance with sampling, processing and/or analysis. W. Cai and W. Zhai provided constructive comments on the manuscript. The Surface Ocean CO<sub>2</sub> Atlas (SOCAT) is an international effort, endorsed by the International Ocean Carbon Coordination Project (IOCCP), the Surface Ocean Lower Atmosphere Study (SOLAS) and the Integrated Marine Biosphere Research (IMBeR) programme, to deliver a uniformly quality-controlled surface ocean CO<sub>2</sub> database. The many researchers and funding agencies responsible for the collection of data and quality control are thanked for their contributions to SOCAT. Comments from three anonymous reviewers significantly improved the quality of this contribution.

## FUNDING

This work was supported by the National Key Scientific Research Project (2015CB954000 and 2015CB954001) sponsored by the Ministry of Science and Technology of China, and by the National Natural Science Foundation of China (91328202).

**Conflict of interest statement.** None declared.

## REFERENCES

- Sabine CL, Feely RA and Gruber N *et al.* The oceanic sink for anthropogenic CO<sub>2</sub>. *Science* 2004; **305**: 367–71.
- Khatiwala S, Primeau F and Hall T. Reconstruction of the history of anthropogenic CO<sub>2</sub> concentrations in the ocean. *Nature* 2009; **462**: 346–9.
- Cai W-J. Estuarine and coastal ocean carbon paradox: CO<sub>2</sub> sinks or sites of terrestrial carbon incineration? *Annu Rev Mar Sci* 2011; **3**: 123–45.
- Holt JT, Harle J and Proctor R *et al.* Modelling the global coastal ocean. *Philos Trans R Soc A* 2009; **367**: 939–51.
- Bonan GB and Doney SC. Climate, ecosystems, and planetary futures: the challenge to predict life in earth system models. *Science* 2018; **359**: eaam8328.
- Regnier P, Friedlingstein P and Ciais P *et al.* Anthropogenic perturbation of the carbon fluxes from land to ocean. *Nat Geosci* 2013; **6**: 597–607.
- Bauer JE, Cai W-J and Raymond PA *et al.* The changing carbon cycle of the coastal ocean. *Nature* 2013; **504**: 61–70.
- Andersson AJ and Mackenzie FT. Shallow-water oceans: a source or sink of atmospheric CO<sub>2</sub>? *Front Ecol Environ* 2004; **2**: 348–53.
- Duarte CM, Middelburg JJ and Caraco N. Major role of marine vegetation on the oceanic carbon cycle. *Biogeosciences* 2005; **2**: 1–8.
- Laruelle GG, Cai W-J and Hu X *et al.* Continental shelves as a variable but increasing global sink for atmospheric carbon dioxide. *Nat Commun* 2018; **9**: 454.
- Borges A, Delille B and Frankignoulle M. Budgeting sinks and sources of CO<sub>2</sub> in the coastal ocean: diversity of ecosystems counts. *Geophys Res Lett* 2005; **32**: L14601.
- Cai W-J, Dai M and Wang Y. Air-sea exchange of carbon dioxide in ocean margins: a province-based synthesis. *Geophys Res Lett* 2006; **33**: L12603.
- Chen C-TA and Borges AV. Reconciling opposing views on carbon cycling in the coastal ocean: continental shelves as sinks and near-shore ecosystems as sources of atmospheric CO<sub>2</sub>. *Deep-Sea Res II* 2009; **56**: 578–90.
- Laruelle GG, Dürr HH and Slomp CP *et al.* Evaluation of sinks and sources of CO<sub>2</sub> in the global coastal ocean using a spatially-explicit typology of estuaries and continental shelves. *Geophys Res Lett* 2010; **37**: L15607.
- Chen C-TA, Huang T-H and Chen Y-C *et al.* Air-sea exchanges of CO<sub>2</sub> in the world's coastal seas. *Biogeosciences* 2013; **10**: 6509–44.
- Dai M, Cao Z and Guo X *et al.* Why are some marginal seas sources of atmospheric CO<sub>2</sub>? *Geophys Res Lett* 2013; **40**: 2154–8.
- Laruelle GG, Lauerwald R and Pfeil B *et al.* Regionalized global budget of the CO<sub>2</sub> exchange at the air-water interface in continental shelf seas. *Glob Biogeochem Cycle* 2014; **28**: 1199–214.
- Bourgeois T, Orr JC and Resplandy L *et al.* Coastal ocean uptake of anthropogenic carbon. *Biogeosciences* 2016; **13**: 4167–85.
- Laruelle GG, Landschützer P and Gruber N *et al.* Global high-resolution monthly pCO<sub>2</sub> climatology for the coastal ocean derived from neural network interpolation. *Biogeosciences* 2017; **14**: 4545–61.
- Cai W-J and Dai M. Comment on 'enhanced open ocean storage of CO<sub>2</sub> from shelf sea pumping'. *Science* 2004; **306**: 1477c.
- Gruber N. Carbon at the coastal interface. *Nature* 2015; **517**: 148–9.
- Cai W-J, Chen L and Chen B *et al.* Decrease in the CO<sub>2</sub> uptake capacity in an ice-free Arctic Ocean basin. *Science* 2010; **329**: 556–9.
- Lohrenz SE, Cai W-J and Chen F *et al.* Seasonal variability in air-sea fluxes of CO<sub>2</sub> in a river-influenced coastal margin. *J Geophys Res* 2010; **115**: C10034.
- Omar AM, Olsen A and Johannessen T *et al.* Spatiotemporal variations of fCO<sub>2</sub> in the North Sea. *Ocean Sci* 2010; **6**: 77–89.
- Zhai W, Dai M and Chen B *et al.* Seasonal variations of air-sea CO<sub>2</sub> fluxes in the largest tropical marginal sea (South China Sea) based on multiple-year underway measurements. *Biogeosciences* 2013; **10**: 7775–91.
- Evans W, Mathis JT and Cross JN *et al.* Sea-air CO<sub>2</sub> exchange in the western Arctic coastal ocean. *Glob Biogeochem Cycle* 2015; **29**: 1190–209.
- Guo X, Zhai W and Dai M *et al.* Air-sea CO<sub>2</sub> fluxes in the East China Sea based on multiple-year underway observations. *Biogeosciences* 2015; **12**: 5495–514.
- Laruelle GG, Lauerwald R and Rotschi J *et al.* Seasonal response of air-water CO<sub>2</sub> exchange along the land-ocean aquatic continuum of the northeast north American coast. *Biogeosciences* 2015; **12**: 1447–58.
- Volta C, Laruelle GG and Regnier P. Regional carbon and CO<sub>2</sub> budgets of North Sea tidal estuaries. *Estuar Coast Shelf Sci* 2016; **176**: 76–90.

30. Chou W-C, Tishchenko PY and Chuang K-Y *et al.* The contrasting behaviors of CO<sub>2</sub> systems in river-dominated and ocean-dominated continental shelves: a case study in the East China Sea and the Peter the Great Bay of the Japan/East Sea in summer 2014. *Mar Chem* 2017; **195**: 50–60.
31. Geilfus N-X, Pind M-L and Else BGT *et al.* Spatial and temporal variability of seawater pCO<sub>2</sub> within the Canadian Arctic archipelago and Baffin Bay during the summer and autumn 2011. *Cont Shelf Res* 2018; **156**: 1–10.
32. Lachkar Z and Gruber N. Response of biological production and air-sea CO<sub>2</sub> fluxes to upwelling intensification in the California and canary current systems. *J Mar Syst* 2013; **109**: 149–60.
33. Mackenzie FT, Lerman A and Ver LMB. Role of the continental margin in the global carbon balance during the past three centuries. *Geology* 1998; **26**: 423–6.
34. Hofmann EE, Cahill B and Fennel K *et al.* Modeling the dynamics of continental shelf carbon. *Annu Rev Mar Sci* 2011; **3**: 93–122.
35. Takahashi T, Olafsson J and Goddard JG *et al.* Seasonal variation of CO<sub>2</sub> and nutrients in the high-latitude surface oceans: a comparative study. *Glob Biogeochem Cycle* 1993; **7**: 843–78.
36. Takahashi T, Sutherland SC and Sweeney C *et al.* Global Sea-air CO<sub>2</sub> flux based on climatological surface ocean pCO<sub>2</sub>, and seasonal biological and temperature effects. *Deep-Sea Res II* 2002; **9–10**: 1601–22.
37. McKee BA, Aller RC and Allison MA *et al.* Transport and transformation of dissolved and particulate materials on continental margins influenced by major rivers: benthic boundary layer and seabed processes. *Cont Shelf Res* 2004; **24**: 899–926.
38. Körtzinger AA. Significant CO<sub>2</sub> sink in the tropical Atlantic Ocean associated with the Amazon River plume. *Geophys Res Lett* 2003; **30**: 2287.
39. Cooley SR, Coles VJ and Subramaniam A *et al.* Seasonal variations in the Amazon plume-related atmospheric carbon sink. *Glob Biogeochem Cycle* 2007; **21**: GB3014.
40. Tseng C-M, Liu K-K and Gong G-C *et al.* CO<sub>2</sub> uptake in the East China Sea relying on Changjiang runoff is prone to change. *Geophys Res Lett* 2011; **38**: L24609.
41. Guo X, Cai W-J and Huang W-J *et al.* Carbon dynamics and community production in the Mississippi River plume. *Limnol Oceanogr* 2012; **57**: 1–17.
42. Redfield AC, Ketchum BH and Richards FA. The influence of organisms on the composition of seawater. In: Hill MN (ed.). *The Sea*. New York: Wiley, 1963, 26–77.
43. Du C, Liu Z and Kao S-J *et al.* Diapycnal fluxes of nutrients in an oligotrophic oceanic regime: the South China Sea. *Geophys Res Lett* 2017; **44**: 11510–8.
44. Rixen T and Ittekkot V. Nitrogen deficits in the Arabian Sea, implications from a three component mixing analysis. *Deep-Sea Res II* 2005; **52**: 1879–91.
45. Cao Z, Dai M and Zheng N *et al.* Dynamics of the carbonate system in a large continental shelf system under the influence of both a river plume and coastal upwelling. *J Geophys Res* 2011; **116**: G02010.
46. Han A, Dai M and Kao S-J *et al.* Nutrient dynamics and biological consumption in a large continental shelf system under the influence of both a river plume and coastal upwelling. *Limnol Oceanogr* 2012; **57**: 486–502.
47. Wu K, Dai M and Li X *et al.* Dynamics and production of dissolved organic carbon in a large continental shelf system under the influence of both river plume and coastal upwelling. *Limnol Oceanogr* 2017; **62**: 973–88.
48. Cao Z, Dai M and Evans W *et al.* Diagnosing CO<sub>2</sub> fluxes in the upwelling system off the Oregon-California coast. *Biogeosciences* 2014; **11**: 6341–54.
49. Martz T, Send U and Ohman MD *et al.* Dynamic variability of biogeochemical ratios in the Southern California current system. *Geophys Res Lett* 2014; **41**: 2496–501.
50. Sambrotto RN, Savidge G and Robinson C *et al.* Elevated consumption of carbon relative to nitrogen in the surface ocean. *Nature* 1993; **363**: 248–50.
51. Li R, Xu J and Li X *et al.* Spatiotemporal variability in phosphorus species in the Pearl River estuary: influence of the river discharge. *Sci Rep* 2017; **7**: 13649.
52. Banse K. Uptake of inorganic carbon and nitrate by marine plankton and the Redfield ratio. *Glob Biogeochem Cycle* 1994; **8**: 81–4.
53. Voss M, Croot P and Lochte K *et al.* Patterns of nitrogen fixation along 10°N in the tropical Atlantic. *Geophys Res Lett* 2004; **31**: L23S09.
54. Foster RA, Subramaniam A and Mahaffey C *et al.* Influence of the Amazon River plume on distributions of free-living and symbiotic cyanobacteria in the western tropical North Atlantic Ocean. *Limnol Oceanogr* 2007; **52**: 517–32.
55. Olson EM, McGillicuddy DJ and Dyrman ST *et al.* The depth-distribution of nitrogen fixation by *Trichodesmium spp.* colonies in the tropical–subtropical North Atlantic. *Deep-Sea Res I* 2015; **104**: 72–91.
56. Subramaniam A, Yager PL and Carpenter EJ *et al.* Amazon River enhances diazotrophy and carbon sequestration in the tropical North Atlantic Ocean. *Proc Natl Acad Sci USA* 2008; **105**: 10460–5.
57. Sohm JA and Capone DG. Zonal differences in phosphorus pools, turnover and deficiency across the tropical North Atlantic Ocean. *Glob Biogeochem Cycle* 2010; **24**: GB2008.
58. Hopkinson CS and Vallino JJ. Efficient export of carbon to the deep ocean through dissolved organic matter. *Nature* 2005; **433**: 142–5.
59. Bakker DCE, Pfeil B and Landa CS *et al.* A multi-decade record of high-quality fCO<sub>2</sub> data in version 3 of the surface ocean CO<sub>2</sub> atlas (SOCAT). *Earth Sys Sci Data* 2016; **8**: 383–413.
60. Revelle R and Suess HE. Carbon dioxide exchange between atmosphere and ocean and the question of an increase of atmospheric CO<sub>2</sub> during the past decades. *Tellus* 1957; **9**: 18–27.
61. Sundquist ET, Plummer LN and Wigley TML. Carbon dioxide in the ocean surface: the homogenous buffer factor. *Science* 1979; **204**: 1203–5.